Glass transition of two-dimensional binary soft-disk mixtures with large size ratios

Rei Kurita* and Eric R. Weeks
Department of Physics, Emory University, Atlanta, Georgia 30322, USA
(Received 14 October 2009; revised manuscript received 19 August 2010; published 8 October 2010)

We simulate binary soft-disk systems in two dimensions and investigate how the dynamics slow as the area fraction is increased toward the glass transition. The "fragility" quantifies how sensitively the relaxation time scale depends on the area fraction, and the fragility strongly depends on the composition of the mixture. We confirm prior results for mixtures of particles with similar sizes, where the ability to form small crystalline regions correlates with fragility. However, for mixtures with particle size ratios above 1.4, we find that the fragility is not correlated with structural ordering, but rather with the spatial distribution of large particles. The large particles have slower motion than the small particles and act as confining "walls" which slow the motion of nearby small particles. The rearrangement of these confining structures governs the lifetime of dynamical heterogeneity, that is, how long local regions exhibit anomalously fast or slow behavior. The strength of the confinement effect is correlated with the fragility and also influences the aging behavior of glassy systems.

DOI: 10.1103/PhysRevE.82.041402 PACS number(s): 83.80.Hj, 64.70.pv, 61.20.Ja, 64.60.My

I. INTRODUCTION

Many liquids can form glasses if they are cooled rapidly, and glassy materials have technological applications such as optical fibers and plastics [1–5]. The origin of the glass transition is still unclear, despite the scientific and technological interests. Much work has examined the dynamical properties of materials near the glass transition. Those studies revealed several important features of supercooled liquids and glasses. For example, upon approaching the glass transition, the structural relaxation time (τ_α) increases by several orders of magnitude without a corresponding growing static correlation length [6,7]. The rate of this increase in τ_α is called fragility and depends on the material [1–5]. For fragile glass formers, τ_α steeply increases for a small decrease in temperature, while for "strong" glass formers, the increase in τ_α requires a larger decrease in temperature. The relaxation time is related to the viscosity, and thus the fragility is an important factor in the ease of processing glass-forming materials. Typically it is desirable to mold a glass-forming material with the viscosity held within a certain range; for fragile materials, this may correspond to a restrictively narrow range of temperature.

Another common observation of materials close to the glass transition is that they often have a broad distribution of local mobility: some regions in a sample relax much faster than other regions. Eventually, molecules in those regions exchange their dynamics, that is, fast regions become slow, and vice versa. This is termed "dynamical heterogeneity" [8–14]. It is known that the characteristic lifetime of these dynamically heterogeneous regions τ_{DH} is longer than τ_α, and the strong divergence of τ_{DH} near a glass transition temperature suggests that heterogeneous dynamics are relevant for understanding the glass transition [4].

A third common feature of materials in the glassy state is that their properties evolve with time, such as the diffusivity of molecules or dielectric susceptibility. This phenomenon is termed "aging" [15–20]. Despite the changing properties, no clear structural changes have been seen; this can be true even if, for example, diffusivity slows by several orders of magnitude [19,20].

While all of these properties have been known for some time and carefully characterized by experiments, the origins of many of them are unclear. To understand the origins, numerical simulations with simple intermolecular interactions are used to study factors controlling the dynamics. These model systems are useful as clear understanding is hindered by the complexity of real materials [21–25]. For the fragility, some simulations show that liquids become less fragile when the polydispersity increases (or a larger size ratio for binary mixtures is used) [22–24]. This has been explained as due to ordering of the sample, which becomes frustrated in polydisperse samples. For example, in two-dimensional (2D) systems, small regions with hexagonal order can form, which correspond to slower dynamics (larger values of τ_α), and thus increasing the polydispersity frustrates formation of these ordered regions and diminishes the fragility [22]. Furthermore, it is reported that particle mobility in those ordered regions is slower than that in randomly structured regions, and it suggests that dynamical heterogeneity is also influenced by local structure [22,25–33].

Those simulations used the polydispersity as a small perturbation frustrating the ordering, that is, with either a small polydispersity or a binary system with the particle size ratio close to 1. However, dynamics in those situations are quite different from highly polydisperse samples. Binary mixtures have two control parameters: the size ratio and the volume fraction ratio of the two components. These lead to complex phase diagrams [34,35] and potentially emergent dynamical properties such as an effective depletion interaction between the large particles in binary hard-sphere systems [36,37]. Our interest is in dense amorphous phases at intermediate size ratios.

In this paper, we simulate the dynamics of binary soft-disk mixture systems with large size ratios and find that the glass transition in large size ratio binary systems can be quite different from that of systems with smaller size differences.

*Present address: Institute of Industrial Science, University of Tokyo, 4-6-1 Komaba, Meguro-ku, Tokyo 153-8505, Japan.

We study the fragility of binary soft-disk mixtures with various size ratios and area fraction ratios. Local ordering is less significant for large size ratio systems. Instead, we see a molecular crowding effect from the large particles [38,39]. Our data suggest that the large particles act as confining walls for the smaller particles, and that confinement effects increase the fragility of such systems by suppressing dynamical heterogeneity. We also investigate aging in large size ratio systems, and again seen an influence of confinement effects due to the large particles. Overall, our results suggest that confinement effects are crucial to describing the dynamics of the glass transition in binary mixtures with large size ratios between the two components.

II. METHOD

We perform two-dimensional Brownian dynamics simulations for binary mixtures composed of large (L) and small (S) soft particles. These simulations are meant to mimic the colloidal glass transition. For the colloidal glass transition, the key control parameter is the volume fraction [7,11,40], and so in our simulations the chief control parameter is the area fraction ϕ. The results of Brownian dynamics simulations are similar to those of molecular-dynamics simulations in dense systems [22,24,41–43]. The particles interact via the purely repulsive Weeks-Chandler-Andersen potential [44]: $U_{ij}=4\epsilon[(\sigma_{ij}/r)^{12}-(\sigma_{ij}/r)^6+1/4]$ for $r<2^{1/6}\sigma_{ij}$; otherwise, $U_{ij}=0$, where $\sigma_{ij}=(\sigma_i+\sigma_j)/2$ and $i,j\in\{L,S\}$. We fix $k_BT/\epsilon=0.04$, so the total area fraction ϕ is our control parameter to approach the glass transition. The mass ratio is $m_L/m_S=(\sigma_L/\sigma_S)^2$ and the length is normalized by σ_S. The total number of particles is $N=N_L+N_S=1024$ (or 4096), where N_L and N_S are the numbers of large and small species, respectively. We generate initial conditions by simulating at $\phi=0.10$ for a long time and expanding the disk sizes to increase ϕ. We confirm that our results do not show initial condition dependence, and our results are also independent on time below $\phi=0.66$, that is, there is no aging observed. Thus, we consider that our binary systems are well mixed and ergodic for $\phi<0.66$.

For certain area fractions for a 2D monodisperse sample, the hexatic order phase can be found, which has orientational order but no long-range positional order [45]. For binary samples with large size ratios, there is apparently little ordering of either type, while for size ratios close to 1, hexatic phases are still subtle to verify. Hence, we calculate an orientation pair-correlation function $g_6(R)/g(R)$, where R is a normalized distance from a particle. $g_6(R)/g(R)$ decays with the power of $R^{-1/4}$ in a hexatic phase for a monodisperse sample [45]. Thus, we classify our samples as liquid (or glassy) when the power of the decay is faster than $R^{-1/4}$ (Fig. 1). We find no hexatic phases for any area fractions ϕ for systems with size ratios $\sigma_L/\sigma_S=1.2$, 1.25, 1.5, 1.75, 2, 2.5, and 3 and area fraction ratios $\phi_L/\phi_S=N_L\sigma_L^2/N_S\sigma_S^2=0.5$, 0.75, 1, 1.5, and 2; these states are indicated by the circles in Fig. 2(a). We confirm that the decay rates of $g_6(R)/g(R)$ in those simulation conditions are quicker than $R^{1/4}$, and thus we are studying liquids (or glasses at higher ϕ). We note that it is known that several crystalline structures exist in three-dimensional (3D) binary sphere suspensions [34,46]. In none of our samples do we observe large hexagonally ordered patches for our simulations, and the small patches that sometimes appear are transient. This is discussed further below.

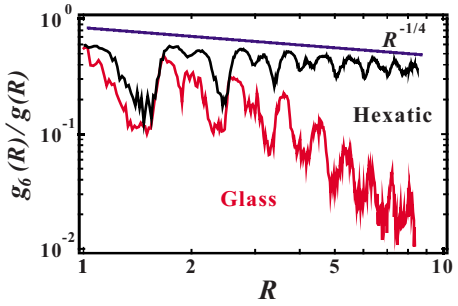

FIG. 1. (Color online) The orientation pair correlation as a function of distance. The straight line corresponds to $R^{-1/4}$, the behavior expected for hexatic phases. A sample with size ratio $\sigma_L/\sigma_S=1.2$ and area fraction ratio $\phi_L/\phi_S=0.5$ at $\phi=0.66$ does not have hexatic order since $g_6(R)/g(R)$ decays faster than the power of $-1/4$ (the lower curve, marked "Glass"). In contrast, the upper curve (marked "Hexatic") shows the correlation for $\sigma_L/\sigma_S=1.15$, $\phi_L/\phi_S=0.5$, and $\phi=0.66$, which has long-range orientational ordering.

When the size ratio is large, a depletion force should be generated [36]. This has been studied before in dilute suspensions of large and small spheres and manifests itself as an effective attractive force between the large spheres [37]. We cannot rule out the existence of the depletion force in our simulations, which may affect the structure of the large particles, although at large area fractions the depletion force may be less relevant. Indeed, we observe pairs of adjacent large particles which are neighbors for long periods of time, but these neighbors separate eventually (see movie S1 of the supplementary material [47]), and in general all of the dy-

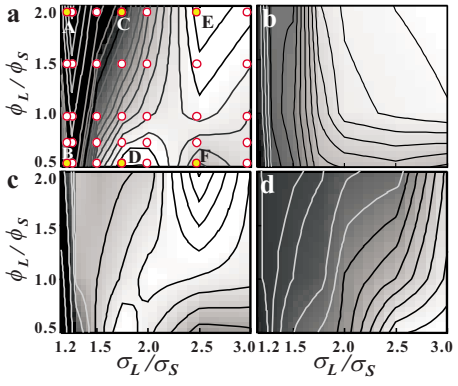

FIG. 2. (Color online) The contour plot of (a) fragility index D, (b) the growth rate of hexagonal order $\partial\langle\psi_6\rangle/\partial\phi$, (c) the growth rate of dynamical correlation length $\partial\xi/\partial\phi$, and (d) the dynamical correlation around a large particle Θ in a plane of $(\sigma_L/\sigma_S,\phi_L/\phi_S)$. All those figures except (a) are obtained at $\phi=0.66$. The shading in each figure is darker when each value is small; thus, the darker regions correspond to (a) fragile liquids, (b) slow growth of hexagonal order, (c) slow growth of dynamical correlation length, and (d) minimal correlations of motion between a large particle and its neighbors. The circles in (a) are the simulated points, and the specific states A–F are labeled.

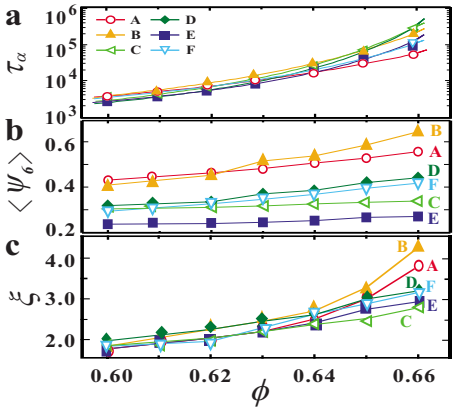

FIG. 3. (Color online) The area fraction ϕ dependence of (a) the relaxation time τ_α, (b) average hexagonal ordering $\langle\psi_6\rangle$, and (c) the dynamic correlation length ξ at states A–F indicated in Fig. 2(a). The solid lines in (a) are fitting lines with the Vogel-Fulcher function at each state. Filled and open symbols correspond to fragile liquids and less fragile liquids, respectively.

namics are slow in our glassy experiments. It is unclear if depletion introduces still slower dynamics or if this is merely part of the overall slow behavior. At least, we note that our systems are quite different from gels with strong attractive force.

III. RESULTS

A. Fragility: Behavior as ϕ increases

We obtain the relaxation time τ_α from the self-part of the intermediate scattering function for all particles, which is given by $F(k,t)=\frac{1}{N}\Sigma_j\langle\exp i\vec{k}\cdot[\vec{r}_j(t)-\vec{r}_j(0)]\rangle$, where $\vec{r}_j$ is the position vector of particle j, $\langle\ \rangle$ indicates a time average, and $\vec{k}$ is the wave vector. τ_α is determined when $F(k_p,\tau_\alpha)=1/e$, where k_p corresponds to the wave number of the first peak of the structure factor. The ϕ dependence of τ_α is well fitted by Vogel-Fulcher function substituting ϕ for $1/T$: $\tau_\alpha=\tau_0\exp[D\phi/(\phi_0-\phi)]$, where D is the fragility index and ϕ_0 is the area fraction of the ideal glass transition [see Fig. 3(a)] [3]. Fragile liquids have smaller values of D. For example, $D\sim4$ for triphenyl phosphite which is one of the most fragile liquids, while for the less fragile liquid butyronitrile, $D\sim30$ [48]. For our simulations, $0.4\lesssim D\lesssim1.0$, smaller than the molecular liquids. The difference may be due to using the density as the control parameter rather than temperature. For comparison, we examined the data of Refs. [49,50] which used light scattering to study the colloidal glass transition as a function of volume fraction. From their data, we find $D=0.497\pm0.002$. Another example is that the fragility index of glycerol in an isothermal experiment is smaller than that measured in an isobaric experiment [51]. We expect our observed qualitative dependence of the fragility on the system parameters to still be revealing.

It is worth noting that, for our data, we also compute the value of D by calculating $F(k,t)$ for only small particles (or large particles), and we obtain almost the same values for D and ϕ_0. We do not see separate glass transitions for the two particle species, which have been seen in simulations with large size ratios and equal particle numbers (thus volume fraction ratios ϕ_L/ϕ_S much larger than ours) [38,39]. In such cases, the large particles do not seem to interact as directly with the small particles but rather have their own glass transition, and then the small particles move in the interstices between the large particles. In our simulations, the volume fraction ratios are somewhat close to 1, and so the large particles always "see" the small particles and the α relaxation time scales for both particle species have similar ϕ dependence.

Figure 2(a) shows the contour plot of the fragility D in a $(\sigma_L/\sigma_S,\phi_L/\phi_S)$ plane. The circles indicate the states simulated. This figure shows that the fragility is a nonmonotonic function of the size ratio or the area fraction ratio. For example, for $\phi_L/\phi_S=2.0$, the fragility has values $D=1.05,0.82,0.45$ for states A, C, and E, but then increases slightly to 0.49 for the state to the right of state E. Likewise, for $\phi_L/\phi_S=0.5$, the fragility behaves nonmonotonically with increasing size ratio: $D=0.64,0.48,0.77$ for states B, D, and F. Comparing states A and B, or states C and D, suggests that increasing the number of large particles increases the fragility index D, but states E and F disprove this trend.

We find that fragile liquids (small D) have small ϕ_0, the area fraction where τ_α appears to diverge. The relationship between fragility and the divergence point of τ_α is observed at glass-forming liquids [52,53], and our results are consistent with them. On the other hand, the existence of ϕ_0 for molecular liquids is still discussed and not well established [54,55]. We are not sure what determines ϕ_0 and why fragility is related to the divergence point. Below, we focus on microscopic properties such as particle mobility and local arrangement.

Prior work observed that two-dimensional systems can form small hexagonally ordered regions, and the mobility of particles is diminished within these regions. More fragile liquids are observed to have large growth rates of the size of these regions with respect to ϕ [22–24]. To check this we study the ϕ dependence of hexagonal order for our samples. We use the local hexatic order parameter described as $\psi_6^j=(1/n_j)|\Sigma_{m=1}^{n_j}e^{i6\theta_m^j}|$, where n_j is the number of nearest neighbors for particle j and θ_m^j is the angle of the relative vector $\vec{r}_m-\vec{r}_j$ with respect to the x axis. $\psi_6^j=1$ means that a hexagonal arrangement is formed around particle j, while $\psi_6^j=0$ corresponds to a nonhexagonal arrangement. We then consider $\langle\psi_6\rangle$, the time and particle average of ψ_6^j. We compare the ϕ dependence of $\langle\psi_6\rangle$ with that of τ_α [Figs. 3(a) and 3(b)]. Both particle sizes are similar at states A and B, $\sigma_L/\sigma_S=1.2$, and here both τ_α and $\langle\psi_6\rangle$ increase dramatically as ϕ increases, suggesting they are indeed related as seen in prior work. However, for states C and E, $\langle\psi_6\rangle$ stays nearly constant with increasing ϕ, while τ_α grows rapidly. The system slows without significant hexagonal ordering.

Next, we compare the fragility with the growth rate of hexagonal ordering $\partial\langle\psi_6\rangle/\partial\phi$ since fragility corresponds to $\partial\log\tau_\alpha/\partial\phi$. (We calculate all derivatives of a quantity X with respect to ϕ as $\partial X/\partial\phi=[X(\phi)-X(\phi-\Delta\phi)]/\Delta\phi$, where we choose $\Delta\phi=0.01$. In the results below, we compare the behavior of the samples at a fixed $\phi=0.66$. However, our

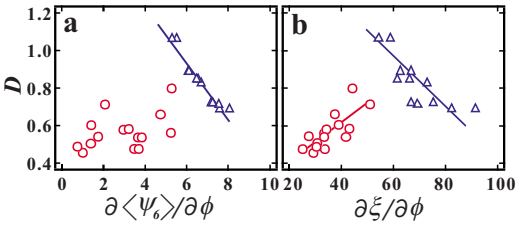

FIG. 4. (Color online) The fragility index D as a function of (a) $\partial\langle\psi_6\rangle/\partial\phi$ and (b) $\partial\xi/\partial\phi$ at $\phi=0.66$. The triangles correspond to systems where size ratio is close to 1 ($\sigma_L/\sigma_S<1.4$), and the circles correspond to large size ratios (>1.4). The lines are added as guides to the eye.

results show similar trends when comparing samples at fixed τ_α.) Figure 2(b) shows the contour plot of $\partial\langle\psi_6\rangle/\partial\phi$ at $\phi=0.66$ in a plane of $(\sigma_L/\sigma_S, \phi_L/\phi_S)$. The growth of hexagonal order is small at large σ_L/σ_S and ϕ_L/ϕ_S (upper right region). This behavior is expected since hexagonal ordering should be frustrated with increasing σ_L/σ_S. Figure 4(a) shows D as a function of $\partial\langle\psi_6\rangle/\partial\phi$. We observe two distinct behaviors. For similar particle size systems ($\sigma_L/\sigma_S<1.4$, triangles), more fragile liquids (smaller D) have a larger dependence of hexagonal order on ϕ, in agreement with prior work [22]. In contrast, large size ratio systems ($\sigma_L/\sigma_S>1.4$, circles) show less correlation between the growth of hexagonal order and the fragility index.

Cooperative motion of groups of particles is a common phenomenon as the glass transition is approached [10–13,56,57], and this behavior is thought to be more common in fragile glasses. Figures 5(a) and 5(c) show snapshots of the systems at $\phi=0.66$ at states B and E, where particles are colored based on Δr_j^2, and groups of highly mobile particles are seen (darker colors). To define displacements, here

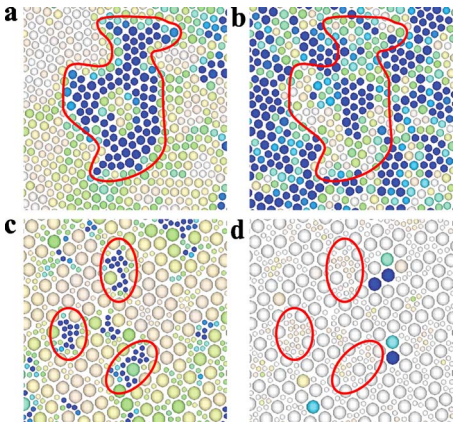

FIG. 5. (Color online) (a) and (b) are snapshots of the system at state B, $\phi=0.66$; (c) and (d) are at state E, $\phi=0.66$. The simulation box is four times as large as those snapshots in each side. In (a) and (c), particles are colored based on mobility Δr_j^2, with darker colors indicating more mobile particles. The darkest color corresponds to $\Delta r_j^2=0.25\sigma_s^2$. The displacement time scale Δt is chosen to maximize the non-Gaussian parameter, and is $\Delta t=5\times10^4$ for (a) and 2×10^4 for (c). In (b) and (d), particles are colored based on the hexagonal order parameter ψ_6^j, with the darkest color corresponding to $\psi_6^j=0.8$. The outlined regions are guides to the eye.

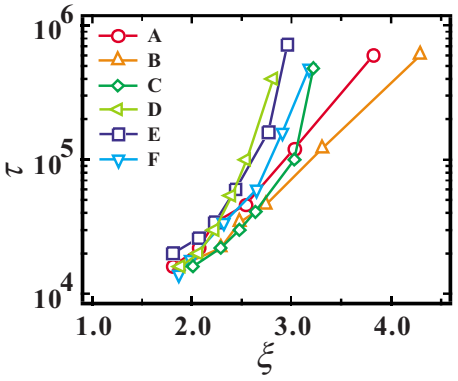

FIG. 6. (Color online) τ_α as a function of ξ for our six representative states. We find two trends of behaviors. One is an exponential correlation for systems with size ratio close to 1 (A and B, $\sigma_L/\sigma_S=1.25$), and the other is a faster divergence of τ_α with ξ for the systems with larger size ratios.

(and for the subsequent analysis in this work) we focus on the time scale Δt^* for which the non-Gaussian parameter is the largest. The non-Gaussian parameter is defined as

$$\alpha_2(\Delta t) = \frac{1\langle\Delta r^4\rangle}{2\langle\Delta r^2\rangle^2} - 1, \tag{1}$$

with displacements Δr measured over the lag time Δt, and the factor of 1/2 is chosen so that $\alpha_2=0$ for a Gaussian distribution [58]. α_2 is larger when the tails of the distribution become broad. Prior work identified the time scale Δt^* that maximizes α_2 as related to cage rearrangements [8,9,11]. In our current work, we computed α_2 separately for the large and small particles, finding similar values for Δt^*. For our analysis, we will use Δt^* based on α_2 calculated for the small particles, and our results are not sensitive to this choice.

Examining our data, we observe clusters with cooperative motion in our systems, some of which are circled in Figs. 5(a) and 5(c). To look for the connection between the cooperative motion and fragility in our sample, we need to characterize the cooperative motion. We compute a correlation function described as $S(R)=\langle\Delta\vec{r}_i\cdot\Delta\vec{r}_j\rangle/\langle|\Delta\vec{r}|^2\rangle$, where R is the distance between particles i and j, and $\Delta\vec{r}_i$ is the displacement of particle i at $\Delta t=\Delta t^*$ [56]. We find that $S(R)$ shows exponential decay with R, which was previously observed in experiments [57] and simulations [56]. This exponential decay yields a decay length ξ, which we plot in Fig. 3(c) as a function of ϕ for our six representative states. While all samples have similar short-ranged cooperative motion at $\phi\approx0.60$, we see a variety of behavior as the glass transition is approached. Figure 6 shows the relationship between τ_α and ξ, and again we find two fairly distinct types of behavior. When the size ratio is close to 1 (states A and B), τ_α increases exponentially with increasing ξ. This is consistent with systems with small polydispersity [22]. On the other hand, τ_α seems to diverge at finite ξ for the large size ratio systems (states C–F). It means that the dynamics slow without increasing cooperative motion. Again, it suggests that the dynamics of supercooled liquid in binary systems is strongly sensitive to the size ratio.

Figure 6 shows the clear distinction between large size ratio systems, and close to monodisperse systems, but the relationship between ξ and the fragility is not clear yet. So we focus on the growth rate of ξ, $\partial\xi/\partial\phi$. This is sensible since the fragility index D relates to the growth of τ_α as ϕ increases. Figure 2(c) shows the contour plot of $\partial\xi/\partial\phi$ in a $(\sigma_L/\sigma_S, \phi_L/\phi_S)$ plane. This plot has a rough qualitative similarity to the fragility [Fig. 2(a)]. Figure 4(b) more directly shows that D is related to $\partial\xi/\partial\phi$, with distinct behaviors for $\sigma_L/\sigma_S<1.4$ systems and $\sigma_L/\sigma_S>1.4$ systems. In $\sigma_L/\sigma_S<1.4$ (triangles), fragile liquids have larger increase in ξ with respect to ϕ, and it is natural that the increase in τ_α is related to this. This is also suggested by experimental studies of colloidal suspensions [11,13,57]. In contrast, the opposite relationship is seen for the large size ratio states [circles in Fig. 4(b)]. The most fragile states (small D) correspond to those where ξ grows least as the glass transition is approached. This unusual behavior seems to be a key result for understanding the fragility of large size ratio binary mixtures.

To further understand the relation between ξ and fragility in large size ratio systems, we consider the dynamical difference between the two particle species. We compute the mean-square displacement $\langle\Delta r^2\rangle$ of large and small species separately at a variety of states, and find that the large particles are always significantly slower than the small particles. We next consider how the motion of small and large particles is coupled. To quantify this, we compute the correlation between the directions of motion of a large particle and its neighboring small particles as $\Theta=\langle(1/n_i)\Sigma_i\cos\theta_{ij}\rangle$, where j indicates a large particle, i is the nearest-neighbor particle for particle j, n_i is the number of these neighbors, θ_{ij} is the angle between $\Delta\vec{r}_i$ and $\Delta\vec{r}_j$, $\Delta\vec{r}_j$ is the displacement of particle j at $\Delta t=\Delta t^*$, and the angular brackets indicate a time average and an average over all large particles j. $\Theta=1$ indicates that particles around a large particle move in the same direction as the large particle on this time scale, while $\Theta=0$ means that their movements are uncorrelated with the large particle. Figure 2(d) shows the contour plot of Θ in the plane of $(\sigma_L/\sigma_S, \phi_L/\phi_S)$. Θ ranges from 0.7 (upper left corner) to 0.4 (lower right corner). Cooperative motion decreases as the size ratio increases and as the number of large particles decreases.

If large particles move slower and small particles move independently of the large ones [the lighter-shaded region in Fig. 2(d)], this suggests that the large particles act as slow-moving walls within the large size ratio systems [38,39]. The small particles are trapped in pores between the large particles [see Fig. 5(c)]. In confined geometries, τ_α can dramatically change compared to an unconfined system at the same temperature and density [59–61]. Confined systems with free surfaces typically have smaller values of τ_α, while those with rigid walls have larger values of τ_α [62]. Our data suggest the latter situation is relevant for our large size ratio systems, that crowding due to the large particles slows the motion of the small particles. This has been seen in prior work [38,39], and here we examine this behavior in more detail.

Here, we suggest the fragility of large size ratio systems may be connected to the "strength" of confinement effects. Less fragile liquids may have more mobile walls, such as state C with a large value of Θ (implying that small and large particles move together). Or, less fragile liquids may have a larger spacing between the large particles, such as state F, with a relatively small value of ϕ_L/ϕ_S; here, they are less confined. In contrast, the more fragile states D and E have small values of Θ and smaller distances between large particles. These systems are ultraconfined, where the spacing between large particles is of order ξ or even smaller, thus limiting $\partial\xi/\partial\phi$.

B. Influences of particle mobility at constant ϕ

We also investigate the relationship between local structure and local mobility in our binary systems. According to prior work, the mobility of particles decreases when the particles are in hexagonally ordered regions (for 2D simulations) [22,25], which is also hinted at in 3D colloidal experiments [26]. Thus, we focus on the spatial distribution of mobility and hexagonal structure. Figure 5(a) shows a snapshot of the system in state B at $\phi=0.66$ with the darker colors indicating particles with larger values of Δr_j^2, and Fig. 5(b) shows the same snapshot coloring the particles by their values of ψ_6^j. The circled regions in Figs. 5(a) and 5(b) show that mobile regions correspond to regions with less ordering. We calculate the Pearson correlation coefficient $C(\Delta r_j^2, \psi_6^j)$, finding $C=-0.13$, supporting the idea that mobility is slightly anticorrelated with hexagonal ordering, consistent with prior work.

For large size ratio systems, we see little hexagonal structure on average [curves E and F in Fig. 3(b)], but this does not preclude the possibility that locally there may be hexagonal ordering which influences the dynamics. To check this, we compare the local mobility with local structure. Figures 5(c) and 5(d) show Δr_j^2 and ψ_6^j for state E, with a much larger size ratio, and here there is no correspondence ($C=0.01$). Overall, for the large size ratio samples ($\sigma_L/\sigma_S>1.4$), we never observe any ordered structures at any area fraction. However, we cannot rule out the possibility that there is subtle ordering that might be present and influencing the dynamics.

Next, we consider the relationship between the confinement effects and mobility in large size ratio systems. The confinement effects are composed of both confinement size effects and confinement surface effects. For confined colloidal suspensions, particle motion was slower in more confined spaces, but there was no strong influence from the confining surfaces [60]. Numerical simulations show that the particles move slowly near rough walls, and quickly near smooth walls [59]. We thus wish to distinguish between finite-size effects and interfacial effects. First, we define clusters of large particles as those large particles separated by a distance less than $1.4\sigma_L$, and these clusters form walls surrounding small particles. In some cases, a connected cluster of large particles completely surrounds a group of small particles, as sketched in Fig. 7. Within such a region, we compute the distance R_w from each small particle to the nearest wall particle. The maximum value of R_w within the confined region defines R_c, the effective "confinement pore size." R_w and R_c are indicated in Fig. 7(a). R_w is calculated per small particle,

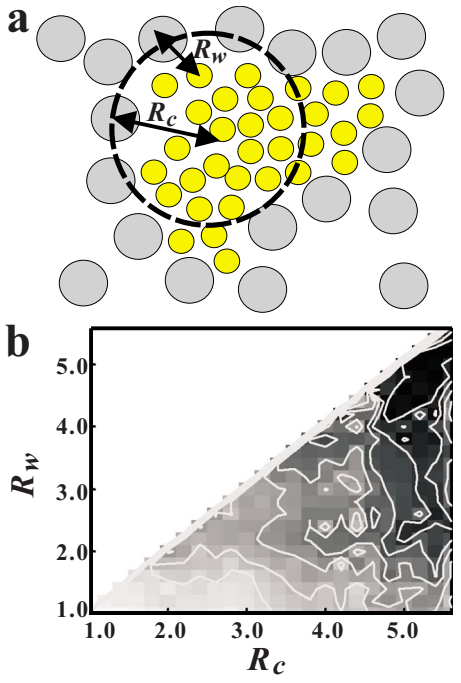

FIG. 7. (Color online) (a) Schematic showing a group of small particles temporarily confined within a region bounded by large particles. Each small particle is assigned a value R_w, which is its closest distance to any large particle (the large particles act as walls). Within each region, the local maximum of R_w identifies the confinement pore size R_c for that region. Thus, R_c is the maximum radius of a circle that fits within the bounded region. (b) A contour plot for the mean-square displacement $\langle \Delta r^2 \rangle$ (at fixed $\Delta t = \Delta t^*$) as a function of the effective pore size R_c where the given particle is located, and the distance of that particle from the nearest wall R_w, for state E with $\phi = 0.66$. Darker shading corresponds to high mobility. The motion of particles is faster in larger pores (large R_c) and when further from the walls (larger R_w for a constant R_c). The length scales are in terms of the small particle diameter. For these data, $R_c^* = 3.6$; only 10% of regions have $R_c > R_c^*$.

and R_c per pore; both of these are functions of time. The dependence of specific particles' behaviors on R_w should give insight into interfacial effects, and the dependence of pore-averaged behavior on R_c should give a separate insight into finite-size effects, although of course these two effects are likely both present simultaneously.

Figure 7(b) shows a contour plot of $\langle r^2 \rangle$ as a function of a (R_w, R_c) plane at state E and $\phi = 0.66$. The results are located only at the lower right of the graph as $R_c \geq R_w$ from our definitions. The darker region at the upper right corresponds to high $\langle r^2 \rangle$, showing that the mobility increases inside large pores (large R_c) and far from walls (large R_w). Given the incommensurate sizes of the large and small particles, it is difficult for small particles to pack well near the walls [see Fig. 5(c)], and so not surprisingly our results are consistent with simulated rough walls [59]. There is also a slight gradient of increasing mobility as a function of pore size R_c for fixed $R_w < 1.5$, indicating that there is a finite-size effect in addition to an interfacial effect. That is, smaller pores (smaller R_c) have more particles close to the pore walls, and thus experience stronger interfacial effects, but the data indicate that the influence of the interface on adjacent particles is less within large pores.

To obtain further evidence for the relationship between the confinement effects and dynamical heterogeneity, we also investigate the temporal relationship between local structures and dynamical heterogeneity. We calculate the intermediate function $F(k, \Delta t)$ for small and large particles separately at fixed $k = 2\pi/\sigma_S$ for small particles [thick solid (black) line in Fig. 8(a)] and $k = 2\pi/\sigma_L$ for large particles [thick dashed (blue) line in Fig. 8(a)]. The structural relaxation time scales for small and large particles, τ_S and τ_L, are set by $F(k, \tau) = 1/e$. We next consider all of the confined regions and the distribution of region sizes R_c. We determine the distribution of all pore sizes R_c (taken over the entire simulation run) and find the threshold size R_c^* for the top 10% of this distribution. For each pore at each time, we define $W_c(t) = 1$ if $R_c(t) > R_c^*$ and $W_c(t) = 0$ otherwise. Typical values of R_c range from 2.8 to 5.6. The temporal correlations of the regions are given by $\langle W_c(\Delta t) W_c(0) \rangle / \langle W_c(0)^2 \rangle$, plotted as the thin solid (red) line in Fig. 8(a). The typical lifetime of large regions is given as τ_c where the correlation drops to $1/e$. Similarly, for each particle we define a parameter W_{DH}, which is equal to 1 if the particle's displacement Δr at that time is within the top 10% of the displacement distribution, and zero otherwise. The correlation $\langle W_{DH}(\Delta t) W_{DH}(0) \rangle / \langle W_{DH}(0)^2 \rangle$ is plotted as the thin dashed (green) line in Fig. 8(a), and τ_{DH} is defined by the $1/e$ time again; this is the time scale over which particles exchange between being fast and slow, as mentioned in the Introduction.

Figure 8(b) shows the ϕ dependence of these time scales (τ_S, τ_L, τ_c, τ_{DH}, and Δt^*). The fastest time scale is τ_S (filled circles), and the large particles are much slower (τ_L, open circles). What is more notable is that $\tau_L \approx \tau_c$; in other words, large particle motions relate to the relaxation of confined regions. This is further evidence that the large particles form walls. Furthermore, $\tau_c \approx \tau_{DH}$ is observed, connecting the confinement-induced dynamics with the dynamically fast particles. Faster particles exchange identities with slower particles when the confining walls rearrange.

If the spatial dynamical heterogeneity is actually induced by the confinement effect, we would expect to see $\tau_L \approx \tau_c \approx \tau_{DH}$, and the correspondence should be strongest for large size ratio systems. Figures 8(c) and 8(d) show these time scales normalized by τ_S as a function of the size ratio σ_L/σ_S at $\phi_L/\phi_S = 2.0$ and 0.5, respectively; the data are for $\phi = 0.66$. Indeed, for $\sigma_L/\sigma_S \geq 1.5$, we find that τ_L is similar to τ_c and τ_{DH}. Not surprisingly, the relaxation time scale τ_c for the confinement effect is governed by the relaxation time τ_L for the large particles which define the pores; more significantly, the lifetime of dynamically heterogeneous regions is also connected to the behavior of the large particles.

On the other hand, we find $\tau_L/\tau_S \to 1$ when $\sigma_L/\sigma_S \to 1$, which is to be expected. In these cases, τ_{DH} remains large, showing that here the dynamical heterogeneity is less influenced by the relaxation of the large particles. However, τ_{DH} is of same order as the lifetime of hexagonal order, as seen in Figs. 8(c) and 8(d) by comparing the triangles (τ_{DH}) with the filled hexagons (τ_{hex}). This new time scale, τ_{hex}, is defined in a similar way as the other time scales: particles with $\psi_6 > 0.8$ are considered hexagonal, and the correlation time for

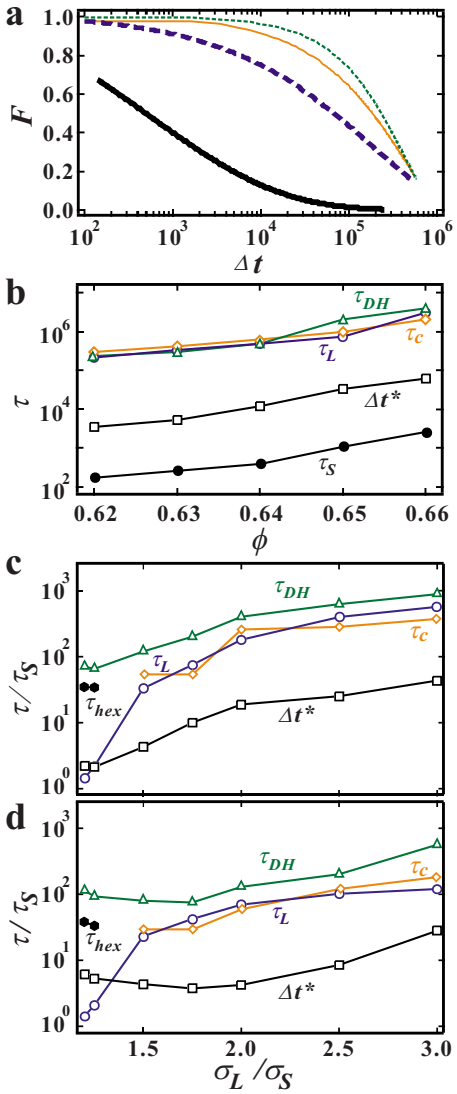

FIG. 8. (Color online) (a) The time dependence of $F(k,\Delta t)$ for small particles [thick solid (black) line; $k=2\pi/\sigma_S$] and for large particles [thick dashed (blue) line; $k=2\pi/\sigma_L$] at state E and $\phi=0.66$. The thin solid (red) line indicates the breakup of the largest confined regions, and the thin dashed (green) line indicates when the most mobile particles become less mobile. (b) The typical structural relaxation time τ_S for small particles (filled circles), the structural relaxation time τ_L for large particles (open circles), the confinement lifetime τ_c (diamonds), the dynamical heterogeneity lifetime τ_{DH} (triangles), and the peak time for the non-Gaussian parameter Δt^* (squares). The data are for state E. (c) Five time scales (τ_L, τ_c, τ_{DH}, Δt^*, and τ_{hex}) normalized by τ_S as functions of σ_L/σ_S at $\phi_L/\phi_S=2.0$ at $\phi=0.66$. τ_{hex} is the lifetime of hexagonal order and corresponds to the filled hexagon symbols. (These data go through state points A, C, and E; see Fig. 2.) (d) Five time scales (τ_L, τ_c, τ_{DH}, Δt^*, and τ_{hex}) normalized by τ_S as functions of σ_L/σ_S at $\phi_L/\phi_S=0.5$ at $\phi=0.66$. (These data go through state points B, D, and F.) There are only a few confinement regions when $\sigma_L/\sigma_S<1.5$, preventing a clear determination of τ_c, so those curves are clipped in (c) and (d).

having $\psi_6>0.8$ is τ_{hex}. This time scale is only relevant for samples with reasonable amounts of hexagonal order [compare Figs. 5(b) and 5(d)], and so is only shown for samples with small size ratios. [This is why it is not shown in Fig. 8(b), which has $\sigma_L/\sigma_S=2.5$.] It is further evidence that local hexagonal order influences the dynamics in similar size ratio systems. In these cases, the confinement effect is more likely due to hexagonal regions composed of both particle species, rather than networks formed by only the large particles, and thus τ_c becomes ill defined and we do not show it in Figs. 8(c) and 8(d).

The competition between hexagonal ordering and crowding due to large particles likely accounts for the cases in Figs. 8(c) and 8(d) where $\tau_{DH}>\tau_L$. For example, states with $\sigma_L/\sigma_S=1.5$ still have regions of hexagonal ordering composed of both particle sizes. In these cases Θ is small [see Fig. 2(d)] and the confinement effect is weak. Another example where $\tau_{DH}>\tau_L$ is the state with $\sigma_L/\sigma_S=3.0$, $\phi_L/\phi_S=0.5$ [Fig. 8(d)]. The large particles are scarce, but result in a strong confinement influence; however, the more numerous small particles can themselves form hexagonal patches, influencing their mobility. We expect that for 3D glass formers, local crystalline order is much less significant, and so confinement effects would more strongly determine τ_{DH} in all cases.

Furthermore, we consider the relationship among Δt^* and other time scales [Figs. 8(c) and 8(d)]. As a reminder, Δt^* is the time scale at which the small particle displacement distribution is the most non-Gaussian. This time scale is used to define the mobility of particles and so is part of the definition of a "mobile" particle and thus τ_{DH}. $\Delta t^*>\tau_S$ shows that small particles move at appreciable distances during the time Δt^*. That is, the non-Gaussian displacements are over significant distances, enough to relax the small particle structure, and this becomes truer at larger size ratios, although this motion is all localized within a region defined by nearby large particles. In all cases $\tau_{DH}>\Delta t^*$ showing that slow and fast regions do not change identities with each particle rearrangement, but rather take longer times to change. Particles may rearrange several times confined within a large pore (several Δt^*) before the pore rearranges and the particles change their mobility. An important caveat is that these observations are for the average behavior of particles, and we are not implying that the connections between pore sizes and dynamics are strongly deterministic. Nonetheless the hierarchy of time scales in Fig. 8 is suggestive of nontrivial connections between the spatial arrangements of the large particles and the long-lived lifetimes of dynamically unusual regions, both fast and slow.

C. Aging

Next we investigate aging dynamics in binary samples with large size ratios. We study state E at $\phi=0.72$ where it is in a glassy state ($\phi_g\sim0.68$ for this state). Figure 9(a) shows $\langle\Delta r^2\rangle$ for small and large species separately at waiting times $t_w=10^3$, 10^4, 10^5, and 10^6. At short time scales ($\Delta t<5000$), $\langle\Delta r^2\rangle$ is independent of t_w. Particles move within cages formed by their nearest-neighbor particles. At longer time scales $\Delta t>5000$, $\langle\Delta r^2\rangle$ increases as the cages rearrange and allow particles to move to new positions. This upturn in $\langle\Delta r^2\rangle$ decreases with increasing t_w, indicating the aging of

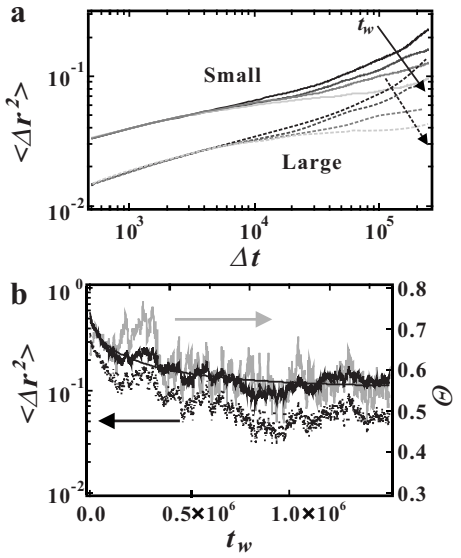

FIG. 9. (a) $\langle \Delta r^2 \rangle$ as a function of lag time Δt for small particles (solid lines) and for large particles (dashed lines) at $t_w = 10^3$, 10^4, 10^5, and 10^6 at state E and $\phi = 0.72$. The mobility of both particle species decreases with respect to aging time. (b) The dark black lines correspond to $\langle \Delta r^2 \rangle$ at $\Delta t = 10^5$ as a function of aging time t_w for small particles (solid) and large particles (dashed). The smooth curves are fits with a stretched exponential, and we find that the decay time of large particles is slightly shorter than that of small particles. The gray line shows the waiting time dependence of Θ, the correlation between the displacements of a large particle and its surrounding small particles. The choice of $\Delta t = 10^5$ is arbitrary although (a) shows that this is a reasonable choice to capture the slowing dynamics.

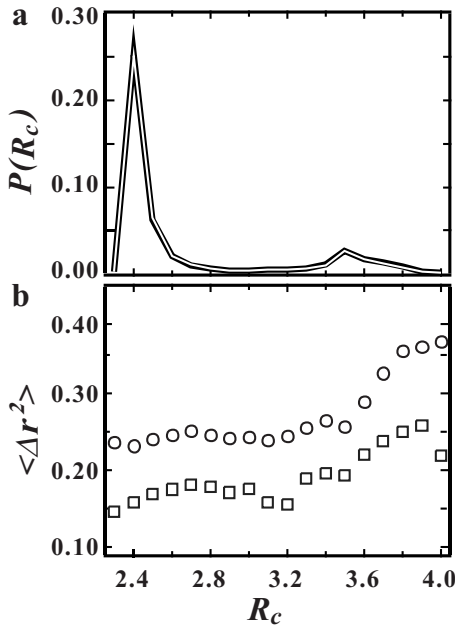

FIG. 10. (a) The probability distribution $P(R_c)$ of confinement pore sizes at $t_w = 10^3$ (black line) and $t_w = 10^6$ (superimposed white line), showing that the distributions are essentially identical. This is for state E with $\phi = 0.72$. (b) Mean-squared displacements $\langle \Delta r^2 \rangle$ for fixed $\Delta t = 10^5$ as a function of the confinement pore size R_c at $t_w = 10^3$ (circles) and $t_w = 10^6$ (squares), for the same state as (a). The upward trend (faster motion for larger pores) is similar to what is seen in equilibrated liquids [Fig. 7(b)]. For these data $\Delta t = 10^5$ to capture time scales over which the dynamics age [see Fig. 9(b)].

the system, similar to what has been seen in experiments [18–20]. Figure 9(b) shows the t_w dependence of $\langle \Delta r^2 \rangle$ at fixed $\Delta t = 10^5$. Although the results at small t_w ($t_w < \Delta t$) are hard to interpret as the dynamics change during Δt, we can observe the clear temporal change of $\langle \Delta r^2 \rangle$ for both particle species. For "old" systems, the plateau of $\langle \Delta r^2 \rangle$ extends over a large range of time scales, with the plateau height corresponding to the cage size. Within our uncertainty, the large and small particles age almost at the same rates, as suggested by the similar shapes of $\langle \Delta r^2 \rangle$ curves [Fig. 9(a)]. Again, these observations are consistent with experiments in binary colloidal glasses [20].

We wish to know a reason for the slowing dynamics with respect to the waiting time. First, we confirm that the overall structure is unchanged with age: we compute the pair-correlation function $g(R)$ at $t_w = 1000$ and 10^6 and cannot observe any difference between them, similar to prior observations in simulations [63] and experiments [19,20]. $g(R)$ is a spatial average over the whole system, so we next consider the relation between local structure and local mobility. We use the confinement pore size R_c to characterize the local structure of the particles within a given confining region. Figure 10 shows $\langle \Delta r^2 \rangle$ and the probability distribution $P(R_c)$, both as functions of R_c at $t_w = 1000$ and 10^6. We find that $P(R_c)$ does not change at all, and this is further evidence that the structure does not change. However, the mobility decreases with age with the dependence on R_c relatively unchanged other than the amplitude. This implies that the mobility decrease is not due to local structural changes, but rather an average slowing of the whole system [19].

Next, we focus on the importance of confinement which strongly influences the dynamics of our equilibrated large size ratio binary systems. As noted above, the confinement strength depends on the confinement size R_c and the effective rigidity of the walls, that is, Θ. In aging systems, $P(R_c)$ does not change with respect to t_w, but Θ could depend on t_w since Θ is a dynamical property rather than a structural property. We compute $\Theta(t_w)$ at fixed $\Delta t = 10^5$, shown as the gray line in Fig. 9(b). The behavior of Θ looks similar to the mobility change of both particles. Figure 11 shows a scatter plot of the mean-square displacement $\langle \Delta r^2 \rangle$ as a function of Θ, for all large particles and all waiting times t_w. We can clearly see the correlation between the mobility and Θ. When Θ decreases, the cooperative motion between small and large particles is less; in other words, the rigidness of walls increases. This result implies that confinement effects become stronger during aging, and it may help to explain the slowing down of the mobility. However, we do not know why Θ decreases as the sample ages.

IV. CONCLUSION

We have examined the glass transition in binary mixtures with a large size ratio, finding results that are distinct from binary mixtures with smaller size ratios. Systems with

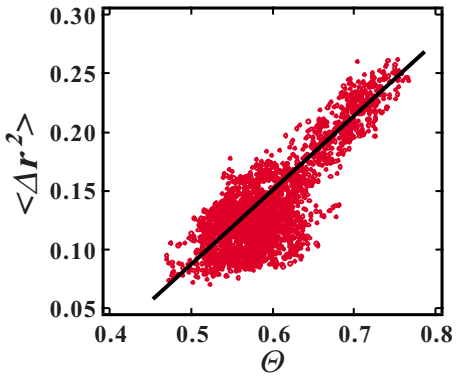

FIG. 11. (Color online) Scatter plot of the mean-square displacement $\langle \Delta r^2 \rangle$ as a function of Θ at state E and $\phi=0.72$, using $\Delta t = 10^5$. Each point corresponds to a different t_w, the time since the start of the simulation. The solid line is a least-squares fit. The data indicate that mobility is linked to the correlation of the motion between large particles and their nearest neighbors.

smaller size ratios are often studied, and the utility of using two particle sizes in those cases is to frustrate the packing and prevent crystallization. Crystals are also frustrated in our simulations with large size ratios, and in addition we find several unique results. First, we have investigated fragility of binary systems. The fragility of binary systems with size ratios close to 1 ($\sigma_L/\sigma_S < 1.4$) is related to the growth of ordered regions: more fragile liquids show dramatic increases in hexagonal order as the glass transition is approached [22–24]. However, systems with larger size ratios do not show this relation. Both types of systems have fragilities which are related to the growth of a dynamical length scale ξ, although the sign of this correlation is opposite for the small and large size ratio systems.

The data show that in large size ratio systems, large particles act as quasi-immobile walls which confine the small particles and slow the dynamics overall. The large particles define regions with a range of sizes. Small particles in large regions find it easier to move, even if within that region they may be adjacent to a large particle at the boundary of the region. Small particles in smaller regions are much less mobile. In addition to these finite-size effects, there are interfacial effects: small particles near large particles move slower than those farther away. Those results are what are often seen in experiments and simulations of confined supercooled liquids. Furthermore, as is often observed in simulations and experiments, we find some particles that are unusually mobile. Our observation is that the length of time which these particles stay unusually mobile is connected to the lifetime of the confinement effect and thus the relaxation time of the large particles.

Finally, we also investigate aging dynamics in large size ratio systems. Below the glass transition, the mobility decreases with respect to the waiting time, although we cannot observe any structural change. We find that in "younger" systems the motion of large particles is correlated with the motion of their neighbors, but that in "older" systems this correlation is markedly smaller. This correlation (or lack of it) relates to the confinement effect, suggesting that the large particles become more rigid confiners in older samples.

It is important to note that simulations of softer particles with a charged (Yukawa) potential find results different from ours, pointing out that our results are not completely generalizable. In simulations with a size ratio of 1:5, the large particles crystallized [46]. In these cases, the large particles did not rearrange but rather moved on their lattice sites, and small particles could only move by diffusive hopping motions between the crystal interstices. This is in contrast to our simulations where the large particles are always able to rearrange (albeit more slowly than the small particles).

Overall, our results suggest that in binary soft-sphere systems, the effect of the large particles to induce finite-size effects within the sample plays an interesting role in the dynamics. Two relevant variables are the finite sizes of regions between large particles and the effective rigidity of the large particles. While our simulation studies 2D systems, the results are similar to prior observations in 3D binary colloidal experiments [20,64] with moderate size ratios. While the effects are easiest to see with large size ratios, one implication of our simulations is that these effects may be relevant although less obvious in binary systems of smaller size ratios. Indeed, one of the goals of our simulations was to understand the effect of structure by using systems where structural heterogeneity is more obvious. These results may also have implications for studies of nanocomposites, where inclusions into polymer glasses can dramatically affect the properties of materials [65,66].

ACKNOWLEDGMENTS

This work was supported by the National Science Foundation under Grant No. DMR-0804174. R.K. was supported by the Japan Society for the Promotion of Science.

[1] P. G. Debenedetti and F. H. Stillinger, Nature (London) **410**, 259 (2001).
[2] C. A. Angell, J. Non-Cryst. Solids **131–133**, 13 (1991).
[3] C. A. Angell, Science **267**, 1924 (1995).
[4] M. D. Ediger, C. A. Angell, and S. R. Nagel, J. Phys. Chem. **100**, 13200 (1996).
[5] J. Horbach, W. Kob, and K. Binder, Philos. Mag. B **77**, 297 (1998).
[6] R. M. Ernst, S. R. Nagel, and G. S. Grest, Phys. Rev. B **43**, 8070 (1991).
[7] A. van Blaaderen and P. Wiltzius, Science **270**, 1177 (1995).
[8] W. Kob, C. Donati, S. J. Plimpton, P. H. Poole, and S. C. Glotzer, Phys. Rev. Lett. **79**, 2827 (1997).
[9] C. Donati, J. F. Douglas, W. Kob, S. J. Plimpton, P. H. Poole, and S. C. Glotzer, Phys. Rev. Lett. **80**, 2338 (1998).
[10] M. D. Ediger, Annu. Rev. Phys. Chem. **51**, 99 (2000).

[11] E. R. Weeks, J. C. Crocker, A. C. Levitt, A. Schofield, and D. A. Weitz, Science **287**, 627 (2000).
[12] M. M. Hurley and P. Harrowell, Phys. Rev. E **52**, 1694 (1995).
[13] L. Berthier *et al.*, Science **310**, 1797 (2005).
[14] R. Yamamoto and A. Onuki, J. Phys. Soc. Jpn. **66**, 2545 (1997).
[15] C. A. Angell, K. L. Ngai, G. B. McKenna, P. F. McMillan, and S. W. Martin, J. Appl. Phys. **88**, 3113 (2000).
[16] I. M. Hodge, Science **267**, 1945 (1995).
[17] W. van Megen, T. C. Mortensen, S. R. Williams, and J. Muller, Phys. Rev. E **58**, 6073 (1998).
[18] R. E. Courtland and E. R. Weeks, J. Phys.: Condens. Matter **15**, S359 (2003).
[19] G. C. Cianci, R. E. Courtland, and E. R. Weeks, Solid State Commun. **139**, 599 (2006).
[20] J. M. Lynch, G. C. Cianci, and E. R. Weeks, Phys. Rev. E **78**, 031410 (2008).
[21] T. Hamanaka and A. Onuki, Phys. Rev. E **74**, 011506 (2006).
[22] T. Kawasaki, T. Araki, and H. Tanaka, Phys. Rev. Lett. **99**, 215701 (2007).
[23] M. Sun, Y. Sun, A. Wang, C. Ma, J. Li, W. Cheng, and F. Liu, J. Phys.: Condens. Matter **18**, 10889 (2006).
[24] D. Coslovich and G. Pastore, J. Chem. Phys. **127**, 124504 (2007).
[25] F. Sausset, G. Tarjus, and P. Viot, Phys. Rev. Lett. **101**, 155701 (2008).
[26] E. R. Weeks and D. A. Weitz, Phys. Rev. Lett. **89**, 095704 (2002).
[27] A. Widmer-Cooper, P. Harrowell, and H. Fynewever, Phys. Rev. Lett. **93**, 135701 (2004).
[28] A. Widmer-Cooper and P. Harrowell, J. Phys.: Condens. Matter **17**, S4025 (2005).
[29] A. Widmer-Cooper, H. Perry, P. Harrowell, and D. R. Reichman, Nat. Phys. **4**, 711 (2008).
[30] J. C. Conrad, F. W. Starr, and D. A. Weitz, J. Phys. Chem. B **109**, 21235 (2005).
[31] G. S. Matharoo, M. S. Gulam Razul, and P. H. Poole, Phys. Rev. E **74**, 050502 (2006).
[32] L. Berthier and R. L. Jack, Phys. Rev. E **76**, 041509 (2007).
[33] G. A. Appignanesi and J. A. R. Fris, J. Phys.: Condens. Matter **21**, 203103 (2009).
[34] A. Imhof and J. K. G. Dhont, Phys. Rev. Lett. **75**, 1662 (1995).
[35] A. D. Dinsmore, A. G. Yodh, and D. J. Pine, Phys. Rev. E **52**, 4045 (1995).
[36] S. Asakura and F. Oosawa, J. Chem. Phys. **22**, 1255 (1954).
[37] J. C. Crocker, J. A. Matteo, A. D. Dinsmore, and A. G. Yodh, Phys. Rev. Lett. **82**, 4352 (1999).
[38] A. J. Moreno and J. Colmenero, Phys. Rev. E **74**, 021409 (2006).
[39] T. Voigtmann and J. Horbach, Phys. Rev. Lett. **103**, 205901 (2009).
[40] P. N. Pusey and W. van Megen, Nature (London) **320**, 340 (1986).
[41] T. Gleim, W. Kob, and K. Binder, Phys. Rev. Lett. **81**, 4404 (1998).
[42] G. Szamel and E. Flenner, EPL **67**, 779 (2004).
[43] M. Tokuyama, Physica A **378**, 157 (2007).
[44] J. D. Weeks, D. Chandler, and H. C. Andersen, J. Chem. Phys. **54**, 5237 (1971).
[45] B. I. Halperin and D. R. Nelson, Phys. Rev. Lett. **41**, 121 (1978).
[46] N. Kikuchi and J. Horbach, EPL **77**, 26001 (2007).
[47] See supplementary material at http://link.aps.org/supplemental/10.1103/PhysRevE.82.041402 for a movie file.
[48] B. Schiener *et al.*, J. Mol. Liq. **69**, 243 (1996).
[49] G. Brambilla, D. El Masri, M. Pierno, L. Berthier, L. Cipelletti, G. Petekidis, and A. B. Schofield, Phys. Rev. Lett. **102**, 085703 (2009).
[50] D. El Masri *et al.*, J. Stat. Mech.: Theory Exp. (2009) P07015.
[51] R. L. Cook *et al.*, J. Chem. Phys. **100**, 5178 (1994).
[52] H. Tanaka, J. Phys.: Condens. Matter **10**, L207 (1998).
[53] R. Kurita and H. Tanaka, Phys. Rev. Lett. **95**, 065701 (2005).
[54] T. Hecksher, A. I. Nielsen, N. B. Olsen, and J. C. Dyre, Nat. Phys. **4**, 737 (2008).
[55] A. Donev, F. H. Stillinger, and S. Torquato, J. Chem. Phys. **127**, 124509 (2007).
[56] B. Doliwa and A. Heuer, Phys. Rev. E **61**, 6898 (2000).
[57] E. R. Weeks, J. C. Crocker, and D. A. Weitz, J. Phys.: Condens. Matter **19**, 205131 (2007).
[58] A. Rahman, Phys. Rev. **136**, A405 (1964).
[59] P. Scheidler, W. Kob, and K. Binder, EPL **52**, 277 (2000); **59**, 701 (2002).
[60] C. R. Nugent, K. V. Edmond, H. N. Patel, and E. R. Weeks, Phys. Rev. Lett. **99**, 025702 (2007).
[61] K. Kim, EPL **61**, 790 (2003).
[62] M. Alcoutlabi and G. B. McKenna, J. Phys.: Condens. Matter **17**, R461 (2005).
[63] W. Kob, J.-L. Barrat, F. Sciortino, and P. Tartaglia, J. Phys.: Condens. Matter **12**, 6385 (2000).
[64] T. Narumi, S. V. Franklin, K. V. Desmond, M. Tokuyama, and E. R. Weeks, e-print arXiv:0911.0702.
[65] P. Rittigstein, R. D. Priestley, L. J. Broadbelt, and J. M. Torkelson, Nature Mater. **6**, 278 (2007).
[66] J. M. Kropka, V. Pryamitsyn, and V. Ganesan, Phys. Rev. Lett. **101**, 075702 (2008).